Acta Crystallographica Section B
Structural Science
ISSN 0108-7681

Classification of stacking faults and their stepwise elimination during the disorder → order transformation of nickel hydroxide

T. N. Ramesh,[a] P. Vishnu Kamath[a]* and C. Shivakumara[b]

[a]Department of Chemistry, Central College, Bangalore University, Bangalore 560 001, India, and [b]Solid State and Structural Chemistry Unit, Indian Institute of Science, Bangalore 560 012, India

Correspondence e-mail: vishnukamath8@hotmail.com

Received 10 November 2005
Accepted 11 April 2006

Nickel hydroxide samples obtained by strong alkali precipitation are replete with stacking faults. The local structures of the stacking faults resemble the stacking patterns of different polytypic modifications that are theoretically possible among the layered hydroxides. This resemblance becomes a basis for the classification of stacking faults into different types. Each type of stacking fault produces a characteristic non-uniform broadening of peaks in the X-ray powder diffraction pattern of nickel hydroxide. *DIFFaX* simulations aid the classification and quantification of stacking faults. Hydrothermal treatment of a poorly ordered nickel hydroxide slurry at different temperatures (338–473 K) and different durations (5–48 h) shows that the stacking faults are removed in a stepwise manner. The as-precipitated sample has 17–20% stacking faults of the $3R_2$ variety, which evolve into the $2H_2$ type at 413 K. The $2H_2$ stacking faults persist up to 443 K. The stacking faults are completely removed only at 473 K. At this temperature an ordered β-$Ni(OH)_2$ phase is observed.

1. Introduction

Nickel hydroxide comprises a hexagonal close packing of OH^- ions in which alternate layers of octahedral sites are occupied by Ni^{2+} ions resulting in a stacking of charge-neutral layers having the composition $Ni(OH)_2$ (Oswald & Asper, 1977). The bonding within the layers is iono-covalent, while along the *c* direction it is van der Waals. Nickel hydroxide has a low solubility product (1.6×10^{-14}; Dobos, 1975) and is generally prepared by precipitation from the solution of a suitable nickel salt using a strong alkali. According to Ostwald (1897), the solid obtained immediately from such a reaction is thermodynamically unstable, with its free energy close to that of the reactants. In an earlier paper (Ramesh *et al.*, 2003), we showed that the nickel hydroxide obtained immediately upon precipitation is highly disordered. Several kinds of structural disorder manifest themselves in nickel hydroxide. They are:

(i) Cation vacancies (Cornilsen *et al.*, 1988, 1990).

(ii) Stacking faults (Delmas & Tessier, 1997; Tessier *et al.*, 1999).

(iii) Turbostratic disorder involving the random rotation of successive layers about the *c*-crystallographic axis (Warren & Bodenstein, 1966; Andreev & Lunström, 1994).

(iv) Interstratification arising due to insertion of water molecules and/or anions part of the way in between the hydroxide layers (Rajamathi *et al.*, 2000).

Interstratification results in a layer composition $[Ni(OH)_{2-x}(H_2O)_x]^{x+}$ or $[Ni(OH)_{2-x}(A^{n-})_{x/n}]$ (Rajamathi *et al.*, 2001). Cation vacancies result in a layer composition $[Ni_{1-x}\square_x(OH)_{2-2x}(H_2O)_{2x}]$. Both these disorders deprive Ni^{2+} of its symmetric coordination. The thermodynamic stability of any

crystalline solid is directly related to the symmetry of the bonding in the first coordination sphere (Verma & Krishna, 1966); a higher symmetry leads to greater thermodynamic stability. Interstratification and cation vacancies adversely affect the stability of nickel hydroxide. Therefore, this badly crystalline material orders itself in two distinct steps (Ramesh *et al.*, 2005), by:

(i) removal of interstratification and cation vacancies at relatively low temperatures (383–413 K) and

(ii) removal of stacking faults at $T > 443$ K.

The elimination of interstratification and cation vacancies restores the preferred coordination of the Ni^{2+} ions. The stacking faults, on the other hand, do not disrupt the first coordination shell of the Ni^{2+} ions and hence persist up to much higher temperatures (443 K).

In this paper we classify and quantify the stacking faults on the basis of their local structures which we call 'motifs'. For this we rely on the stacking patterns of the different polytypic modifications that are theoretically possible for a layered hydroxide (Bookin & Drits, 1993). As the different polytypes differ from one another in their thermodynamic stability, so do the stacking faults. The elimination of stacking faults during the ordering of nickel hydroxide should therefore be a complex process, and in this paper we also examine the exact mechanism by which the layers restack in an ordered sequence. This study is important as earlier work has correlated the charge storage capacity of nickel hydroxide to the extent of structural disorder (Ramesh *et al.*, 2005). Among the various kinds of disorder, stacking faults are the most important determinators of superior electrochemical performance.

We were therefore interested in understanding the nature and origin of stacking faults in nickel hydroxide. While in a simple layered material such as graphite the stacking faults can be generated by the translation of randomly selected layers by (1/3, 2/3, z) or (2/3, 1/3, z), the stacking faults in nickel hydroxide are more complex. Using upper-case symbols A, B and C to represent hydroxyl ion positions and lower case symbols a, b and c to represent cation positions, a typical metal hydroxide layer can be represented as AbC or AC. Crystalline nickel hydroxide is expected to have the stacking sequence $AC\,AC\,AC\ldots$. This is represented by the symbol $1H$ (Bookin & Drits, 1993) to denote the single-layered periodicity of a hexagonal lattice. However, the precipitation phenomenon does not preclude the formation of other hydroxide layers AB, BC, CA,... and their insertion into the primary $1H$ stacking sequence. These layers are related to each other by translations, reflections or their combinations. For instance, layer BA is related to AC by a (1/3, 2/3) translation, while layer CB is related to AC by a (2/3, 1/3) translation. CA is related to AC by a mirror-plane reflection, while AB is related to AC by a combination of translation and reflection. Insertion of these various layers into the primary sequence generates different interlayer sites. For instance, the insertion of an AB layer into the primary sequence generates only octahedral interlayer sites, while the insertion of CA layers generates only trigonal prismatic interlayer sites, and insertion of a BA layer generates an octahedral site on one side and a trigonal prismatic site on the other. We show in this paper how the presence of different types of stacking faults affects the X-ray powder diffraction pattern of nickel hydroxide in distinct ways.

2. Experimental

Alkali-induced precipitation of nickel hydroxide at a constant high pH was carried out as described elsewhere (Jayashree *et al.*, 2000) by the slow addition (rate 4 ml min^{-1}) of a nickel nitrate solution (1 M, 50 ml) to a reservoir of NaOH (2 M, 100 ml) at 353 $\pm$ 5 K under constant stirring. The slurry thus obtained was aged in mother liquor for 18 h at 338 K and we label this sample as 18NH338. In separate experiments, freshly precipitated slurries were hydrothermally treated for durations t ranging from 5 to 48 h at different temperatures T ranging from 383–473 K. The samples are labeled as tNHT.

All samples were characterized by X-ray powder diffraction using a Siemens D5005 powder X-ray diffractometer. Data were collected with a Cu $K\alpha$ source (Ni filter, $\lambda = 1.541$ Å) at a scan rate of 2° 2θ min^{-1} and were rebinned into steps of 0.05° 2θ. The powder diffraction pattern of the Si standard yielded an instrumental contribution to the broadening in the range 0.15–0.2° 2θ over 77–28° 2θ.

3. *DIFFaX* simulations

For the successful simulation of the X-ray powder diffraction patterns by *DIFFaX* (Treacy *et al.*, 1991, 2000), the following data have to be input into the program.

3.1. Layer structure

The cell parameters (a = 3.12, c = 4.61 Å) and atomic position parameters of $Ni(OH)_2$ were obtained from a Rietveld refinement of the X-ray powder diffraction pattern of a crystalline sample (space group $P\bar{3}m1$). The positions are Ni (0, 0, 0); O1 (−1/3, −2/3, −0.2257) and O2 (1/3, 2/3, 0.2257). The position parameters of all the symmetry-related atoms were explicitly provided and the point-group symmetry was declared as unknown. Such an option enables the *DIFFaX* code to compute the Laue symmetry. Table 1 gives some of the essential parameters input into the *DIFFaX* simulations.

3.2. Line shape

The calculated Bragg reflections are broadened by using a suitable line-shape function to facilitate comparison with the observed pattern. A Lorentzian was chosen for this purpose. As *DIFFaX* is not a profile-refinement program and only enables a qualitative comparison of the experimental and calculated patterns, the use of a Lorentzian profile function is adequate and has been successful in the past (Ramesh *et al.*, 2003). The FWHM value of the Lorentzian is 0.3° in 2θ for all computations where no comparison with experimental patterns is intended. Where a comparison with an experimental pattern is intended, the FWHM of the Lorentzian is chosen to be the same as that of the peak due to the 100 reflection. The 100 reflection is unaffected by any disorder and

Table 1
Input parameters for the *DIFFaX* simulation of the X-ray powder diffraction pattern of nickel hydroxide.

Cell parameters: a = 3.12; c = 4.60 Å. Point-group symmetry: unknown. Disc diameter: infinite.

Site	x	y	z
A	−1/3	−2/3	0.2257
B	0	0	0
C	1/3	2/3	−0.2257

	Stacking vector		
Transitions	x	y	z
$AC \rightarrow AC$	0	0	1
$AC \rightarrow CB$	2/3	1/3	1
$AC \rightarrow BA$	1/3	2/3	1

is broadened only by crystallite size effects. For a layered material such as $Ni(OH)_2$, crystallite size can be measured along the *ab* plane as the disc diameter and along the *c*-crystallographic axis as the thickness. A small disc diameter selectively broadens the 100 reflection and the choice of this FWHM value for the Lorentzian obviates the need to explicitly include the crystallite size in the simulation.

3.3. Stacking vector

The lattice is constructed by stacking the layers one above another. The use of the stacking vector (0, 0, 1) yields the perfectly crystalline $1H$ lattice. For the purpose of this study, the $1H$ polytype is considered the primary structure and any departure from the stacking sequence of $1H$ is termed as a fault. To generate the $2H$ stacking fault motifs, two different layers were defined. For instance, to generate the $2H_2$ type of stacking faults, two different layers, AC and AB, were defined and stacked one on top of the other by using the stacking vector (0, 0, 1). The probabilities $P_{ACAC} = P_{ABAB}$ and $P_{ACAB} = P_{ABAC}$ ($P_{ACAB} = 1 - P_{ACAC}$) were varied until a good match between the simulated and observed patterns was obtained. The former value gives the relative abundance of the $1H$ polytypic motifs while the latter gives the relative abundance of the $2H_2$ type of stacking faults. The $2H_1$ stacking faults are similarly generated by defining AC and CA layers. The $2H_3$ stacking faults are generated by defining AC and BA layers. To generate the $3R_2$ type of stacking faults, three layers AC, BA and CB were defined and stacked one on top of the other by using the stacking vector (0, 0, 1). The probabilities $P_{ACAC} = P_{BABA} = P_{CBCB}$ give the relative abundance of the $1H$ motifs, while $P_{ACBA} = P_{BACB} = P_{CBAC}$ yield the relative incidence of the $3R_2$ stacking-fault motifs. $P_{ACCB} = P_{BAAC} = P_{CBBA}$ are set equal to zero. To generate the $3R_1$ stacking-fault motifs, $P_{ACBA} = P_{BACB} = P_{CBAC}$ was set equal to zero, while $P_{ACCB} = P_{BAAC} = P_{CBBA}$ was varied. The goodness of the simulation is judged by calculating the reliability factor R_{wp} (Young, 1993). A value of R_{wp} in the range 0.08–0.10 was considered acceptable. At such values of R_{wp} a visual examination of the error function showed the absence of any systematic residual intensities in the difference graphs. Wherever prismatic interlayer sites are generated, the interlayer distance is increased to 5.13 Å in order to maintain the HO–OH contact distance at that observed in the crystal.

4. Results and discussion

Bookin & Drits (1993) were the first to examine all the theoretically possible stacking sequences among the layered hydroxides and classify them on the basis of the interlayer sites generated. While the primary stacking sequence $AC\ AC\ AC\ldots$ ($1H$) has a one-layer periodicity, three distinct stacking sequences can be envisaged for a crystal with a two-layer periodicity,

(i) $AC\ CA\ AC\ldots 2H_1$,
(ii) $AC\ AB\ AC\ldots 2H_2$,
(iii) $AC\ BA\ AC\ldots 2H_3$.

Of these, $2H_1$ generates only prismatic interlayer sites, $2H_2$ only octahedral and $2H_3$ an equal number of prismatic and octahedral interlayer sites. Among the sequences with a three-layer periodicity, two have rhombohedral symmetry, of which the $3R_1$ sequence generates only prismatic and the $3R_2$ generates only octahedral interlayer sites,

(iv) $AC\ CB\ BA\ AC\ldots 3R_1$,
(v) $AC\ BA\ CB\ AC\ldots 3R_2$.

Among the hexagonal sequences with a three-layer periodicity, one each generate octahedral and prismatic interlayer sites while the others generate a mix of both interlayer sites.

Among these various polytypes, those most relevant to nickel hydroxide are $1H$, $2H_2$ and $3R_2$ as all these include only octahedral interstitial sites and have the same packing fraction. They can therefore be expected to have similar enthalpies of formation. Fig. 1 shows the *DIFFaX*-simulated X-ray powder diffraction patterns of these three polytypes. The

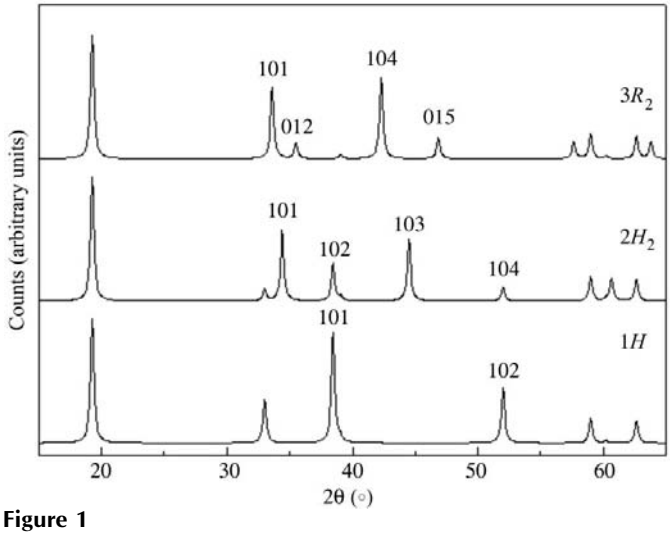

Figure 1
DIFFaX-simulated powder XRD patterns of pure $1H$, $2H_2$ and $3R_2$ polytypes of nickel hydroxide.

polytypes can be distinguished from one another by the positions and relative intensities of their $h0\ell/0k\ell$ reflections.

Disorder can be introduced by a random intergrowth of the three polytypes within the same crystal. The small probability of one polytypic motif in another comprises stacking faults (Prasad & Srivastava, 1971), and provides us with a method of classifying the stacking faults on the basis of their motifs. Furthermore, *DIFFaX* simulations help in their quantification. Crystals with such planar disorders are expected to be stable compared with the ordered crystals (Verma & Krishna, 1966).

In keeping with these expectations, no ordered nickel hydroxide phase of the $2H_2$ and $3R_2$ variety has yet been reported. All nickel hydroxide samples produced by a variety of precipitation reactions (Hui *et al.*, 1995; Zhaorong *et al.*, 1998) exhibit reflections similar to that of the $1H$ polytype. Nevertheless, these reflections are extensively and non-uniformly broadened. The non-uniform broadening of reflections in the X-ray powder diffraction patterns of $Ni(OH)_2$ has been a subject of numerous investigations (Delmas & Tessier, 1997; Tessier *et al.*, 1999; Casas-Cabanas *et al.*, 2005) and it is now accepted that the selective broadening of the $h0\ell$ reflections is on account of stacking faults.

The presence of different types of stacking faults influences the line shape of the $h0\ell$ reflections in different ways. Fig. 2(*a*) shows the *DIFFaX*-simulated X-ray powder diffraction pattern of the $1H$ polytype incorporating stacking faults corresponding to the $2H_2$ motifs. While the 001, 100 and 110 reflections remain unaltered, the 101 and 102 reflections are considerably broadened even at a low (15%) incidence of stacking faults. The broadening of the $h0\ell$ reflections is pronounced at the base. The peak maxima are sharp with 'wings' flaring out at the base. However, at a higher incidence (>20%) the 102 reflection narrows down again with the wings merging into the background, and the 101 reflection is split (not shown). On the incorporation of different proportions of $3R_2$-type stacking faults, a drastic broadening of the 102 reflection is observed [for 30% $3R_2$, see Fig. 2(*b*)]. The peak due to the 101 reflection is also broadened and its intensity falls below that of the 100 reflection. The local structures of the stacking faults are shown as insets in Fig. 2.

Tessier *et al.* (1999) refer to the $2H_2$ type of stacking faults as growth faults and the $3R_2$ as deformation faults (Casas-Cabanas *et al.*, 2005). We feel that our terminology and classification, arising as it does from a crystal chemical viewpoint, is more evocative of the local structure about the fault.

In Fig. 3 we examine the effect of the incorporation of stacking faults corresponding to $2H_1$ and $3R_1$ motifs, respectively. These motifs introduce trigonal prismatic interlayer sites and thereby increase the interlayer distance. In both cases there is a slight broadening of the (001) reflection essentially due to the aperiodicity introduced along the stacking direction, an effect similar to that of interstratifica-

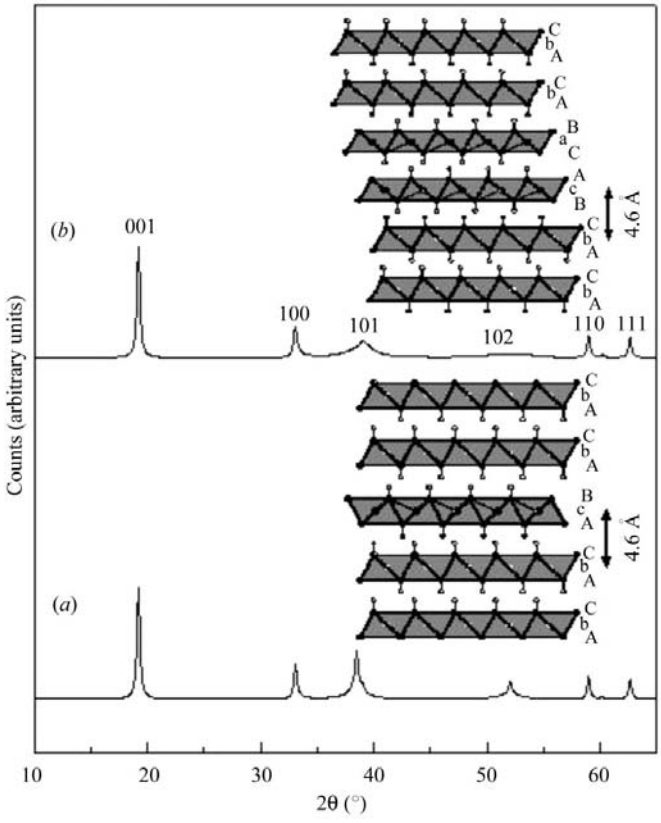

Figure 2
DIFFaX-simulated powder XRD patterns of nickel hydroxide incorporating stacking faults with (*a*) 15% of $2H_2$ and (*b*) 30% of $3R_2$ motifs in the $1H$ polytype. Insets show the local structures of the stacking faults.

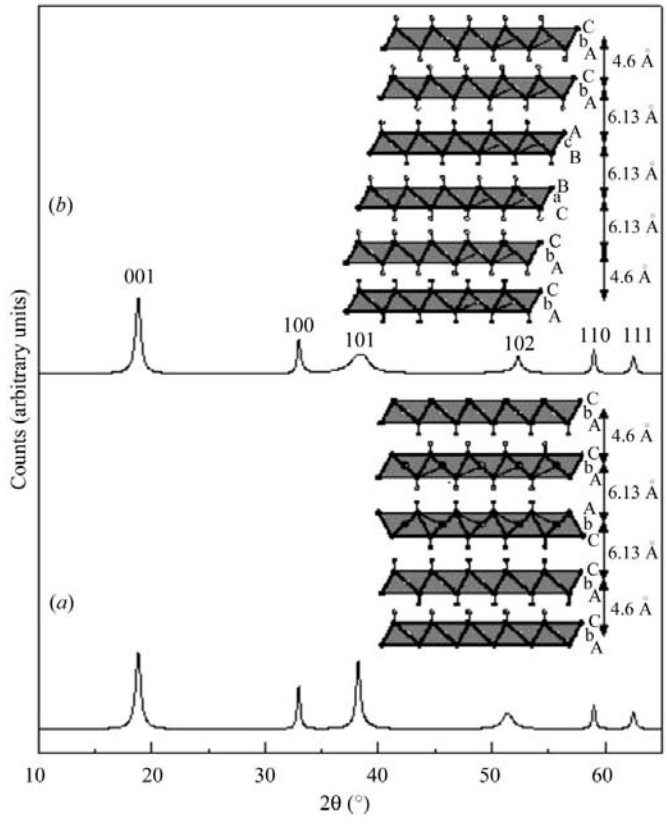

Figure 3
DIFFaX-simulated powder XRD patterns of nickel hydroxide incorporating stacking faults with (*a*) 20% of $2H_1$ and (*b*) 20% of $3R_1$ motifs in the $1H$ polytype. Insets show the local structures of the stacking faults.

Table 2
Effect of different stacking faults on the X-ray powder diffraction pattern of nickel hydroxide.

Ordered crystal		Faulted crystal		
Polytype	Laue symmetry	Stacking fault motif	Laue symmetry	Reflection most affected
$1H$	$\bar{3}m$	–	$\bar{3}m$	–
$2H_1$	6/*mmm*	$2H_1$	6/*mmm*	102
$2H_2$	6/*mmm*	$2H_2$	6/*mmm*	101, 102
$2H_3$	$\bar{3}m$	$2H_3$	$\bar{3}m$	102
$3R_1$	$\bar{3}m$	$3R_1$	$\bar{3}m$	101
$3R_2$	$\bar{3}m$	$3R_2$	$\bar{3}m$	102

tion. The prismatic interlayer sites are stabilized when the interlayer is occupied, as for instance in α-nickel hydroxide (Oliva *et al.*, 1982), where water molecules are intercalated between the hydroxide sheets. α-Nickel hydroxide is thought to crystallize in the $3R_1$ modification. There have been many suggestions of the possible intergrowth of the α motifs in the matrix of β-Ni(OH)$_2$ (Rajamathi *et al.*, 2000). The planar faults arising from the insertion of the $2H_1$ and $3R_1$ motifs are very selective in the way they affect the $h0\ell$ reflections. While the introduction of the $2H_1$ motifs selectively broadens the 102 reflection, leaving the 101 reflection unaffected (Fig. 3*a*), the $3R_1$ motifs have the opposite effect. They drastically broaden the 101 reflection, leaving the 102 reflection relatively unaffected (Fig. 3*b*).

The effect of various types of stacking faults on powder X-ray diffraction (XRD) patterns of nickel hydroxide are summarized in Table 2.

4.1. Disorder → order transformation of nickel hydroxide

In the light of the results obtained in the preceding section, we examine the nature of stacking faults and the mechanism of their elimination in laboratory-synthesized nickel hydroxide samples. The as-precipitated 18NH338 sample has been adequately described in our earlier work (Ramesh *et al.*, 2003) and is replete with interstratification and turbostratic disorder. The elimination of these disorders by hydrothermal treatment has been dealt with in an earlier paper (Ramesh *et al.*, 2005). The effect of stacking faults on the X-ray powder diffraction pattern of nickel hydroxide begins to manifest itself after the elimination of interstratification.

The 18NH383 has only residual interstratification, and in Fig. 4 we illustrate our simulation technique. The observed pattern exhibits non-uniform broadening of lines besides a near total extinction of the 102 reflection. In a stepwise manner, the different faults are built in, into the simulation:

(i) Incorporation of 11% interstratification brings about a satisfactory visual match of the calculated 001 peak with that of the observed pattern (Fig. 4*a*). However, the other reflections, chiefly 100 and 10ℓ (ℓ = 1, 2), do not match, indicating the existence of other types of disorder. The difference profile exhibits systematic residual intensities at Bragg angles corresponding to the 101 and 102 reflections.

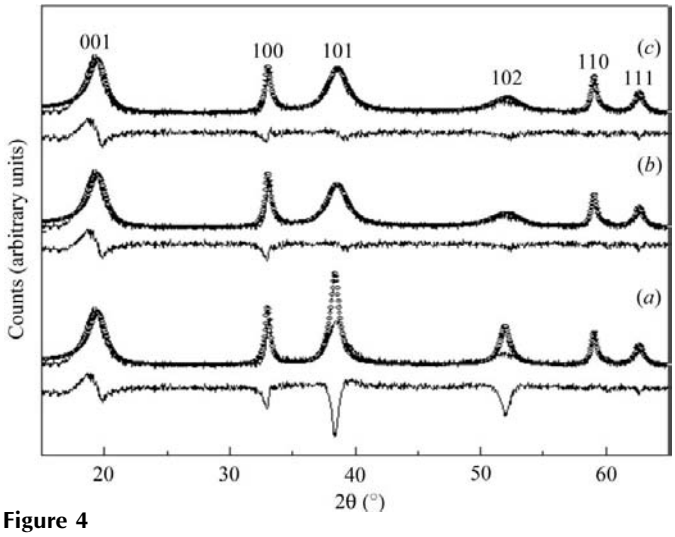

Figure 4
Comparison of simulated (circles) with the observed (solid line) powder XRD patterns of 18NH383 sample: (*a*) nickel hydroxide simulated with 11% interstratification; (*b*) as (*a*) but with 15% $3R_2$ stacking faults; (*c*) as (*b*) but with 17% cation vacancies. The respective difference profiles are also plotted.

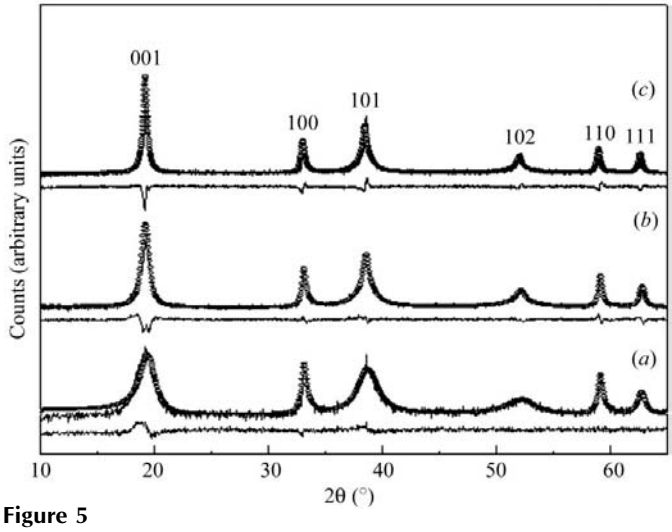

Figure 5
Comparison of simulated with observed powder XRD patterns of (*a*) 5NH413, (*b*) 18NH413 and (*c*) 48NH413. Observed: solid line; simulated: closed circles. The respective difference profiles are also plotted.

(ii) Incorporation of 15% of the $3R_2$ type of motifs brings about a satisfactory match of the 101 and 102 reflections (Fig. 4*b*).

(iii) Incorporation of 17% cation vacancies completes the simulation (Fig. 4*c*).

The X-ray powder diffraction patterns of other samples have been similarly simulated and the results are given in Table 3. It is evident from the simulations that crystal growth is promoted on hydrothermal treatment and there is a progressive growth in particle size with t and T. Furthermore, all the samples obtained in the temperature range 338–398 K, t = 18 h and 413 K at low time (t = 5 h; Fig. 5*a*) have 17–20% of the $3R_2$ type of stacking faults.

The $3R_2$ variety of stacking faults are generated whenever two successive layers in the Ni(OH)$_2$ lattice are related to each

Table 3
Results of *DIFFaX* simulations of the X-ray powder diffraction patterns of different nickel hydroxide samples.

Sample	Crystallite thickness (Å)	Interstratification (%)	Stacking faults (%)		Cation vacancies (%)	Laue symmetry	*R*-weighted pattern (R_{wp})
			$3R_2$	$2H_2$			
18NH338	–	23	20	–	17	$\bar{1}$	0.118
18NH383	–	11	15	–	17	$\bar{1}$	0.082
18NH398	92	–	5	18	17	$\bar{3}m$	0.073
48NH398	369	–	–	17	10	6/*mmm*	0.099
5NH413	–	11	17	–	17	$\bar{1}$	0.076
18NH413	124	–	–	20	14	6/*mmm*	0.076
48NH413	369	–	–	18	10	6/*mmm*	0.139
18NH443	4590	–	–	4	3	6/*mmm*	0.102
48NH443	Infinite	–	–	1.5	1	6/*mmm*	0.117
48NH473	Infinite	–	–	–	–	$\bar{3}m$	0.111

other by the vector (1/3, 2/3, 1). It can be seen that such a translation generates only octahedral interlayer sites so that the close packing of hydroxyl ions of the system is preserved.

The $3R_2$-type stacking faults are eliminated only at $T \geq 413$ K, and we show in Fig. 5 the X-ray powder diffraction patterns observed as a function of time *t*. While at $t = 5$ h the $3R_2$ type of stacking faults can be seen, at $t = 18$ h the line shape of the 102 reflection has broad wings with a narrow maximum, a shape characteristic of the $2H_2$ stacking faults (Fig. 5*b*). A successful simulation of the X-ray powder diffraction pattern of 18NH413 could be realised by the inclusion of 20% $2H_2$-type stacking faults. The $2H_2$ stacking faults continue to persist indefinitely (*t* up to 48 h) at 413 K.

Stacking faults generated by the random insertion of *AB* or *BC* layers into the primary stacking sequence of $1H$ are known as the $2H_2$ type of stacking faults. Since all samples obtained at $T = 413$ K, $t = 18$–48 h, have $2H_2$ stacking faults, it would appear that the $3R_2$ stacking-fault motifs evolve into $2H_2$ stacking-fault motifs as

$$\underbrace{AC\,AC\,AC\,BA\,CB\,AC\,AC\ldots}_{3R_2\ \text{motif}} \rightarrow \underbrace{AC\,AC\,AC\,AB\,AC\,AC\ldots}_{2H_2\ \text{motif}}.$$

The faulted layer *BA* transforms into *AB* either by a non-rigid rotational motion or by a sequence of translations and rigid rotational motions. Our measurements focus on the end products of the transformation process rather than the transformation process itself. At 413 K the $2H_2$ motifs exist indefinitely.

Other authors (Deabate *et al.*, 2000) have tried to explain the non-uniform broadening of the Bragg peaks in the X-ray powder diffraction pattern of nickel hydroxide within the Rietveld formalism. The Rietveld method is more suited to the study of ordered phases and does not permit the explicit inclusion of disorder in the model structure. However, the effect of strain on the X-ray powder diffraction profile can be included in the Rietveld method. Disorder introduces strain in the crystal and the inclusion of strain in the Rietveld refinement procedure offers a way of indirectly evaluating the effect of structural disorder on the powder pattern. The microstrain introduced by Deabate *et al.* (2000) in fact corresponds more closely to interstratification than stacking faults. Stacking faults are, however, more important as they are the primary determinators of the superiority of the electrochemical performance of nickel hydroxide.

The *DIFFaX* approach, while being semiquantitative, is nonetheless superior in the present context as it enables the study of faulted crystals and the systematic engineering of different kinds of structural disorder. The other feature of *DIFFaX* is its ability to evaluate the Laue symmetry of the system being studied. Accordingly the Laue symmetry of the $1H$ and $3R_2$ polytypes is evaluated to be $\bar{3}m$ and that of the $2H_2$ as 6/*mmm*, in keeping with the expectations. While admittedly the inclusion of structural disorder destroys crystal symmetry, stacking faults are special as the introduction of stacking faults does not destroy the symmetry along the stacking direction (Verma & Krishna, 1966). The Laue symmetry of the faulted crystals is also given in Table 2. The inclusion of even a small number of $2H_2$ motifs within the $1H$ polytype enhances the Laue symmetry of the crystal to 6/*mmm*, while the inclusion of $3R_2$ motifs leaves the symmetry unaffected.

Verma & Krishna (1966) have argued that polytypes having a higher symmetry have greater thermodynamic stability. Extending these arguments to faulted crystals, crystals having

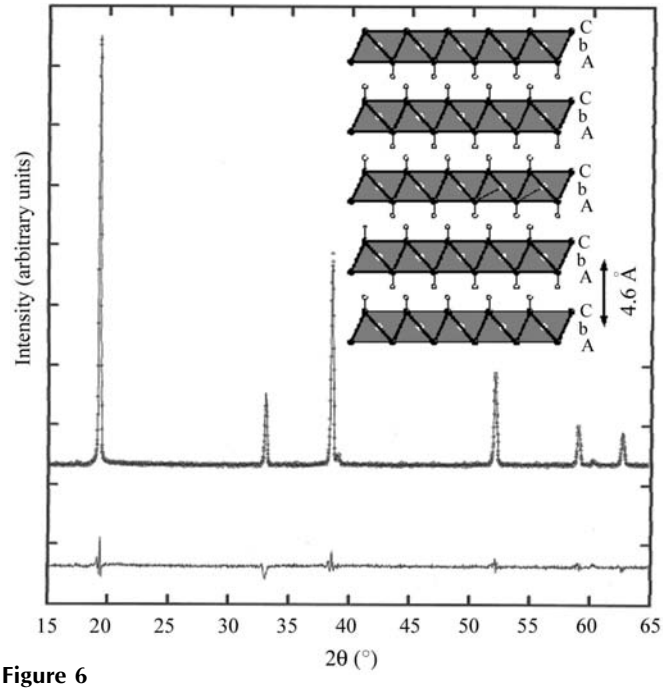

Figure 6
Result of the Rietveld refinement of the powder XRD pattern of 48NH473 nickel hydroxide. Observed: open circle; refined: solid line. The lower trace is the error function. The inset shows the ideal structure of nickel hydroxide.

the $2H_2$ type of stacking faults are expected to have a higher thermodynamic stability compared with those with $3R_2$-type stacking faults. These expectations are in agreement with our observations which show that at 413 K the $3R_2$ type of stacking faults transform into the $2H_2$ type. The $2H_2$ type of stacking faults persist even up to 443 K. A much higher energy regime has to be accessed ($T \simeq 473$ K) before the $2H_2$ stacking faults can be eliminated completely. In Fig. 6 we show the powder X-ray diffraction pattern of 48NH473. The crystallinity of the sample is now adequate to perform a Rietveld refinement with an acceptable difference profile.

5. Conclusion

The evolution of structural order in a poorly ordered nickel hydroxide preparation is a multi-step process. Of particular significance are the stacking faults which persist up to 443 K. From a study of the line shapes in the XRPD patterns, we conclude that the stacking faults present at $T < 413$ K are of the $3R_2$ variety. Above 413 K, stacking faults of the $2H_2$ variety evolve. At $T \simeq 473$ K, all stacking faults are eliminated resulting in the formation of ordered β-$Ni(OH)_2$.

PVK thanks the Department of Science and Technology, Government of India (GOI), for financial support. TNR thanks the Council of Scientific and Industrial Research, GOI, for the award of a Senior Research Fellowship (NET).

References

Andreev, Y. G. & Lunström, T. (1994). *J. Appl. Cryst.* **27**, 767–771.
Bookin, A. S. & Drits, V. A. (1993). *Clays Clay Miner.* **41**, 551–557.
Casas-Cabanas, M., Palacin, M. R. & Rodriguez-Carvajal, J. (2005). *Powder Diffr.* **20**, 334–344.
Cornilsen, B. C., Karjala, P. J. & Loyselle, P. L. (1988). *J. Power Sources*, **22**, 351–357.
Cornilsen, B. C., Shan, X. & Loyselle, P. L. (1990). *J. Power Sources*, **29**, 453–456.
Debabate, S., Fourgeot, F. & Henn, F. (2000) *J. Power Sources*, **87**, 125–136.
Delmas, C. & Tessier, C. (1997). *J. Electrochem. Soc.* **7**, 1439–1443.
Dobos, D. (1975). *Electrochemical Data: A Handbook for Electrochemists in Industry and Universities*, pp. 221–224. Amsterdam: Elsevier.
Hui, L., Yunchang, D., Jiongliang, Y. & Zeyun, W. (1995). *J. Power Sources*, **57**, 137–140.
Jayashree, R. S., Kamath, P. V. & Subbanna, G. N. (2000). *J. Electrochem. Soc.* **147**, 2029–2032.
Oliva, P., Leonardi, J., Laurent, J. F., Delmas, C., Braconnier, J. J., Figlarz, M., Fievet, F. & de Guibert, A. (1982). *J. Power Sources*, **8**, 229–255.
Ostwald, W. (1897). *Z. Phys. Chem.* **22**, 289–330.
Oswald, H. R. & Asper, R. (1977). *Bivalent Metal Hydroxides in Preparation and Crystal Growth of Materials with Layered Structures*, edited by R. M. A. Leith, Vol. 1, pp. 71–170. Amsterdam: Riedel.
Prasad, R. & Srivastava, O. N. (1971). *J. Appl. Cryst.* **4**, 516–521.
Rajamathi, M., Kamath, P. V. & Seshadri, R. (2000). *J. Mater. Chem.* **10**, 503–506.
Rajamathi, M., Thomas, G. S. & Kamath, P. V. (2001). *Proc. Indian Acad. Sci. (Chem. Sci.)*, **113**, 671–680.
Ramesh, T. N., Jayashree, R. S. & Kamath, P. V. (2003). *Clays Clay Miner.* **51**, 570–577.
Ramesh, T. N., Kamath, P. V. & Shivakumara, C. (2005). *J. Electrochem. Soc.* **152**, 806–810.
Tessier, C., Haumesser, P. H., Bernard, P. & Delmas, C. (1999). *J. Electrochem. Soc.* **146**, 2059–2067.
Treacy, M. M. J., Deem, M. W. & Newsam, J. M. (2000). *DIFFaX*, Version 1.807; http://www.public.asu.edu/~mtreacy/DIFFaX.html.
Treacy, M. M. J., Newsam, J. M. & Deem, M. W. (1991). *Proc. R. Soc. London Ser. A*, **433**, 499–520.
Verma, A. R. & Krishna, P. (1966). *Polymorphism and Polytypism in Crystals*, pp. 33–60. New York: John Wiley.
Warren, B. E. & Bodenstein, P. (1966). *Acta Cryst.* **20**, 602–605.
Young, R. A. (1993). *The Rietveld Method.* IUCr/New York: Oxford University Press.
Zharong, C., Gongan, L., Yujuan, Z. & Yunchang, D. (1998). *J. Power Sources*, **74**, 252–254.